Role of interface in optimisation of polyamide-6/Fe3O4 nanocomposite properties suitable for induction heating. [Dataset]

GUPTA, R., PANCHOLI, P.V., YU, X., GUPTA, L., STENNING, G.B.G., BUCKNALL, D., FLYNN, D. and PANCHOLI, K.

2023

Supplementary Data

Role of Interface in optimisation of Polyamide-6/Fe₃O₄ Nanocomposite Properties suitable for Induction Heating

Ranjeetkumar Gupta[1*#], Pinakin V Pancholi[8], Xiangyan Yu[6], Gavin B. G. Stenning[3], L.Gupta[9], David Flynn[5], David Bucknall[4], Ketan Pancholi[1,2*]

[1]School of Engineering, Robert Gordon University, Aberdeen AB10 7GJ, U.K.
[2] Advanced Materials Group, School of Engineering, Robert Gordon University, Aberdeen, AB10 7GJ, U.K.
[3]ISIS Neutron and Muon Source, STFC Rutherford Appleton Laboratory, Didcot OX11 0QX, U.K.
[4]Institute of Chemical Sciences, School of Engineering & Physical Sciences, Heriot-Watt University, Edinburgh EH14 4AS, U.K.
[5]James Watt School of Engineering, University of Glasgow, Glasgow G12 8QQ, U.K.
[6] School of Engineering and Materials Science, Queen Mary University of London, Mile End Road, London, E1 4NS, U.K.
[7]Engineering Development - Process Modelling, National Composites Centre, Bristol & Bath Science Park, Emersons Green, Bristol BS16 7FS, U.K.
[8] Chemistry Department, Gujarat College, Ahmedabad, Gujarat, India, 380006
[9]Quality and Assurances Department, Krishna Enterprises, Sector-69, HSIIDC IMT, Faridabad 121004,
[#]Currently working at – [7]

[*]Corresponding author: k.pancholi2@rgu.ac.uk (K. Pancholi), ranjeet.gupta@nccuk.com (R. Gupta),

Section 1 (S1): Characterisation Methods in detail.

1.   FTIR-ATR

The nanocomposite samples were characterized using Perkin-Elmer ATR-FTIR (Attenuated Total Reflection- Fourier Transmission Infrared Spectroscope) Spectrum Gx system containing DGS-KBr sensor to identify phases and structural changes after addition of the iron oxide NPs. In order to scan each sample, the nanocomposite films of approximately 0.1 mm thickness were prepared and total 30 scans in range of 525-4000 cm-1 wavelength were carried out at a resolution of 4 cm-1. The gain was set to 2 whereas the optical velocity was fixed to 0.4747 m/s.

2.   DSC

DSC was performed using a TA Instruments DSC Q100 at a heating rate of 10°C/min under a nitrogen environment with a temperature range of 20 to 270°C using a sample mass of 9 mg. The Heat/Cool/Heat standard cycle type analysis was selected for accurately depicting the behavior and T_g and T_m for the samples prepared. The running segment consisted of a ramp heating at 10 °C/min to 250 °C, then ramp cooling at 5 °C/min to -90 °C and finally ramp heating at 10 °C/min to 250 °C. The glass transition temperature (T_g) and melting temperature (T_m) were determined from the DSC traces obtained, where the first small endothermic peak represents the glass transition temperature, and the second larger endothermic peak represents the melting temperature of the nanocomposite sample.

3.   XRD

A PANalytical X'Pert Pro MPD, powered by a Philips PW3040/60 X-ray generator and fitted with an X'Celerator detector was used. Diffraction data is acquired by exposing samples to Cu-Kα X-ray radiation, which has a characteristic wavelength (λ) of 1.5418 Å. X-rays were generated from a Cu anode supplied with 40 kV

and a current of 40 mA. The data were collected over a range of 0 to 80° (2θ) with a step size of 0.117o (2θ) and nominal time per step of 1099.82, using the scanning X'Celerator detector. Fixed anti-scatter and divergence slits of 0.38 mm were used together with a beam mask of 10mm and all scans were carried out in a continuous' mode. Phase identification was carried out by means of the X'Pert-PRO accompanying software program PANalytical High Score Plus in conjunction with the JCPDS card.

4. TEM

TEM images were used to determine the morphology and mean diameter in the MNP agglomerates. TEM imaging was conducted at an accelerating voltage of 100 kV, with a spot size of 10 nm. The exposure time was varied from 0 to 50 s. The images of all samples were obtained using a Philips CM100 TEM at different direct magnifications, ranging from x7900 to x245000. An ultrathin section of nanocomposite obtained using microtome were placed on gilder grid of 400 mesh to obtain all images. For NPs imaging, the particles were dispersed in isopropyl alcohol and droplet were placed on TEM grid.

5. SAXS/WAXS

SAXS and WAXS scattering patterns were obtained on Xenocs Nano-inXider, equipped with microfocus sealed tube: Cu, 30W =, point focus. With Dectris Pilatus 3 hybrid photon counting (two fixed) detectors for continuous and simultaneous SAXS and WAXS acquisition up to 2θ=60°. The beam path was windowless beam path, entirely under vacuum from beam delivery system to detector sensor. The SAXS patterns were obtained over a scattering vector length within the range of 0.008 Å^{-1} < q < 0.18 Å^{-1} and WAXS patterns with the range of 0.18 Å^{-1} < q < 0.24 Å^{-1}. One-dimensional (1D) fitting of the scattering curves were obtained by an azimuthal binning and averaging of corresponding two-dimensional scattering patterns using the XSACT (X-Ray Scattering Analysis and Calculation Tool) supplied with the instruments.

All obtained spectra were corrected for background scattering before any further analysis.

$$I(q) = G \exp\left(-\frac{q^2 R_g^2}{3}\right) \qquad \text{Eqn. 1}$$

herein, G is the Guinier pre-factor and R_g the radius of gyration. The Guinier plot represented in Figure of Supplementary Data S5, of Ln I(q) vs q^2, is used to calculate the slope of the chosen region that dictates the value of R_g, giving out the NP/agglomerate size qualitatively.
The NPs are assumed as perfect sphere and the diameter D is calculated with the Equation 2 (2):

$$D = 2 \times (5/3)^{1/2} R_g \qquad \text{Eqn. 2}$$

The slope of regions in the Guinier plot were calculated to give the R_g estimate (3), this was used to calculate the diameters of the NP/agglomerate using Equation 2.

6. Magnetic characterisation

Magnetization loops of the synthesised PNC samples were measured at T = 100K and 400K on Quantum Design MPMS XL-7, integrated with Superconducting Quantum Interference Device (SQUID) detection system and precision temperature control unit. The instrument had temperature range of 1.8 to 400 K and applied maximum field strength of ±7 Tesla with filed uniformity of 0.01% over 4 cm.

Section 2 (S2): Size calculation from TEM images, Degree of Crystallinity calculation and Crystallite size calculation.

In order to measure the average diameter of nanoparticles using TEM images, the obtained TEM images were first converted to 8-bit images and subsequently, the particle analysis was performed to identify the approximated

area of particles assuming them to be circular. The diameters of the particles calculated using relation $\sqrt{(4 \times Area)/\pi}$ were compared with the measured ferret diameters and the average difference between two values were found to be 7.52% with ferret diameters being always smaller.

The enthalpy of all the samples were calculated using the Universal Analysis software that comes along with the DSC instrument control package. By quantifying the heat associated with the melting endotherm. This heat was then reported in terms of percent crystallinity by normalizing the observed heat of fusion with that of the 100% crystalline PA6 polymer. The area used for the enthalpy (crystallinity) calculation as identified using the "Integrate Peak" functionality of the TA Universal Analysis 2000 software is recreated in the plot (included in the main text). The same analysis also helped identify the "Melt Peak Temperature" of the endotherm peak, which was the melting point T_m of the samples and listed in the Table below. Adding to the discussion, the Glass transition temperature T_g was also identified using the "Glass/Step transition" functionality available in the same software.

The degree of crystallinity for all the samples was calculated from the following Equation 3, using the standard reference value of PA6 as cited in the main text.

$$Sample\ Degree\ of\ Crystallinity = \frac{Sample\ Enthalpy\ from\ DSC\ plot}{PA6\ Enthalpy\ from\ Reference\ Text} \times 100\%$$

The following are the observed values for all the samples and the calculated degree of crystallinity for each.

Table S1: A list of degree of crystallinity, Glass transition (T_g) and Melting temperature (T_m) from DSC results for Pristine PA6 sample, PMC sample with uncoated MNPs, PMC samples with varying proportions of silica coatings (Stöber and TPRE) on the MNPs and PMC samples with varying proportions of OA coatings (22 w/w % and 55 w/w%) on the MNPs.

Sample	T_g (°C)	T_m (°C)	Enthalpy (J/g)	Degree of Crystallinity (%)
Pristine PA6	46.35 ± 1	214.15± 2	89.43 ± 2	47.07 ± 2
Uncoated-Fe$_3$O$_4$ PMC	46.22 ± 4	213.32 ± 4	88.95 ± 5	46.81 ± 5
Stöber-Fe$_3$O$_4$ PMC	45.40 ± 2	211.70 ± 2	83.87 ± 4	44.14 ± 4
TPRE-Fe$_3$O$_4$ PMC	45.96 ± 1	209.93 ± 2	87.37 ± 3	45.98 ± 3
22 w/w% OA-Fe$_3$O$_4$ PMC	42.74 ± 2	200.24 ± 3	106.7 ± 4	56.15 ± 4
55 w/w% OA-Fe$_3$O$_4$ PMC	44.15 ± 1	208.34 ± 2	80.46 ± 2	42.34 ± 2

The FWHM values of prominent XRD peaks were used to measure crystallite size of MNPs by using Debye–Scherer formula. The XRD plot peaks were analysed for the crystallite size calculation and the obtained values are summarised as below:

Table S2: Crystallite sizes of MNPs calculated from FWHM of intense peaks observed in XRD patterns for PMC sample with uncoated MNPs, PMC samples with varying proportions of silica coatings (Stöber and TPRE) on the MNPs and PMC samples with varying proportions of OA coatings (22 w/w % and 55 w/w%) on the MNPs.

Sample Type	Absolute Crystallite Size	
	Size(A°)	Size(nm)
Uncoated-Fe$_3$O$_4$ PMC	418 ± 3	42 ± 3
Stöber- Fe$_3$O$_4$ PMC	365 ± 5	37 ± 5
TPRE- Fe$_3$O$_4$ PMC	331 ± 4	33 ± 4
22 w/w% OA-Fe$_3$O$_4$ PMC	300 ± 3	30 ± 3
55 w/w% OA-Fe$_3$O$_4$ PMC	424 ± 13	42 ± 13

Section 3 (S3): SAXS and WAX (small and wide-angle X-ray scattering)

Windowless beam path was used completely under vacuum from beam delivery systems to detector sensors. The SAXS graphs were attained over range of 0.008 Å^{-1}< q < 0.18 Å^{-1} for scattering vector length and range of 0.18 Å^{-1}< q < 0.24 Å^{-1} for WAXS patterns. Azimuthal binning and averaging of corresponding two-dimensional scattering pattern were used for attaining one-dimensional (1D) fitting of the scattering curve supplied XSACT (X-Ray Scattering Analysis and Calculation Tools) with the instruments.
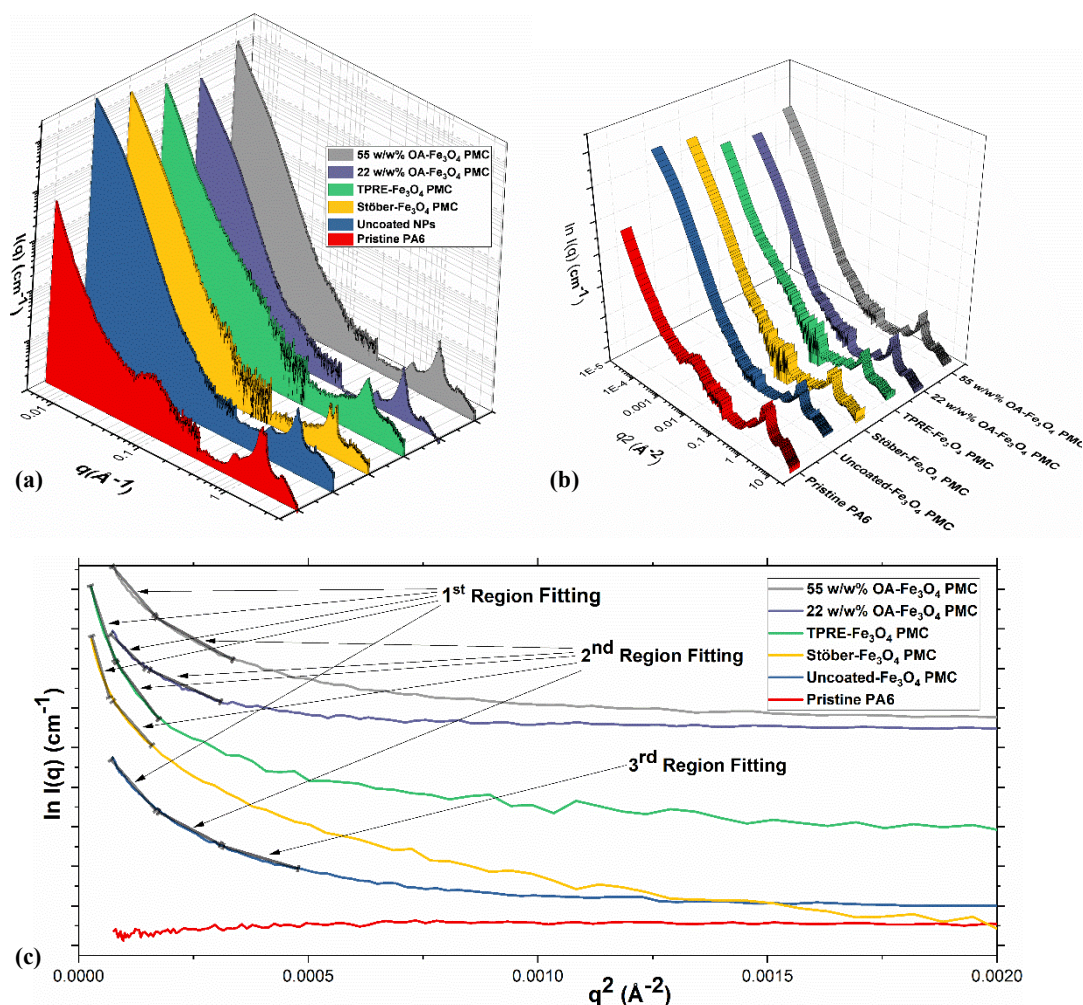

Figure S1. (a) Background corrected SAXS (0.005-0.3 Å^{-1}) and WAXS (0.3-4.17 Å^{-1}) intensities I(q) as a function of the scattering vector 'q' for the pristine polymer (PA6), PMC sample with uncoated MNPs, samples with varying proportions of silica coatings (Stöber and TPRE) on the MNPs, and PMC samples with varying proportions of OA coatings (22 w/w % and 55 w/w%) on the MNPs; (b) Guinier plot for the pristine polymer (PA6), sample with uncoated MNPs, samples with varying proportions of silica coatings (Stöber and TPRE) on the MNPs, and , and samples with varying proportions of OA coatings (22 w/w % and 55 w/w%) on the MNPs; (c) Guinier plot with the region fitting highlighted for the pristine polymer (PA6), sample with uncoated MNPs, samples with varying proportions of silica coatings (Stöber and TPRE) on the MNPs , and samples with varying proportions of OA coatings (22 w/w % and 55 w/w%) on the MNPs.

Firstly, the background corrected SAXS (0.005-0.3 Å^{-1}) and WAXS (0.3-4.17 Å^{-1}) intensities I(q) as a function of the scattering vector 'q = (4π/λ sin θ), where λ is the wavelength of the radiation and θ is one half of the scattering angle.' is plotted in Fig. S2 (a). The Guinier plot represented in Fig. S2 (b), of Ln I(q) vs q^2, is used to calculate the slope of the chosen region that dictates the value of R_g, giving out the MNP/agglomerate size qualitatively. The MNPs are assumed as perfect sphere and the diameter D is calculated using Equation 1 {{88 Hino, Kazuyuki 2008;}}:

$$D = 2 \times (5/3)^{1/2} R_g$$
<div align="right">Eqn. 1</div>

The slope of regions in the Guinier plot were calculated to give the R_g estimate {{89 a 2019;}}, this was used to calculate the diameters of the MNP/agglomerate using Equation 1.

The SAXS profile of the Guinier type plot in Fig. S2 (c), illustrates two vivid areas. One which is flat region because of base polymer response (as can be seen in Pristine PA6 data plot); second, a very steep sloped curve is observed that is related to the response from MNPs in prepared samples. In Fig. S2 (c), the cumulatively slope-dropping area is attributed to the Porod scattering response from MNPs {{51 Porod, G 1982}}. Here, the Guinier area leads the Porod region, in which the former scattering shows the radius of MNPs gyration present in the observed PMC sample as per Guinier's law. Table S3 shows the calculated MNPs average diameters in a PMC volume from the calculation of radius of gyration.

In Table S3, the calculated average MNPs diameter from the SAXS data are in broad agreement with the values obtained from the TEM micrographs, as discussed earlier. The measured values from SAXS/WAXS study confirm that the *22 w/w% OA-Fe₃O₄ PMC Sample* has the smallest mean diameter of MNP/agglomerates. Furthermore, the WAXS curves suggests that some of the bands related to the PA6 crystalline lattices become sharper for functionalised samples, which conforms that the degree of crystallinity changed due to functionalisation. Also, peak height decreases for *Uncoated-Fe₃O₄ PMC Sample* in comparison to the *Pristine PA6 Sample*, highlighting the drop in crystallinity due to MNPs nano-inclusion.

Table S3: Size calculation of the MNPs for each sample types from Guinier plot.

		Uncoated-Fe₃O₄ PMC	*Stöber- Fe₃O₄ PMC*	*TPRE- Fe₃O₄ PMC*	*22 w/w% OA-Fe₃O₄ PMC*	*55 w/w% OA-Fe₃O₄ PMC*
1st Region Fitting	*I(q)* Range	0.009-0.012	0.009-0.014	0.009-0.013	0.009-0.014	0.009-0.012
	R_g	196.719	162.18	186.53	151.19	185.14
	D(nm)	50.79	40.28	46.38	39.04	47.80
2nd Region Fitting	*I(q)* Range	0.012-0.018	0.014-0.021	0.013-0.021	0.014-0.021	0.012-0.019
	R_g	143.985	96.38	146.59	94.06	121.68
	D(nm)	37.17	24.54	38.89	24.29	31.41
3rd Region Fitting	*I(q)* Range	0.018-0.022	-	-	-	-
	R_g	97.123	-	-	-	-
	D(nm)	25.08	-	-	-	-
Observed Range	*D(nm)*	38±13	32±8	42±4	31±8	39±9

Section 4 (S4): Full Scale Magnetisation Plot and calculations.
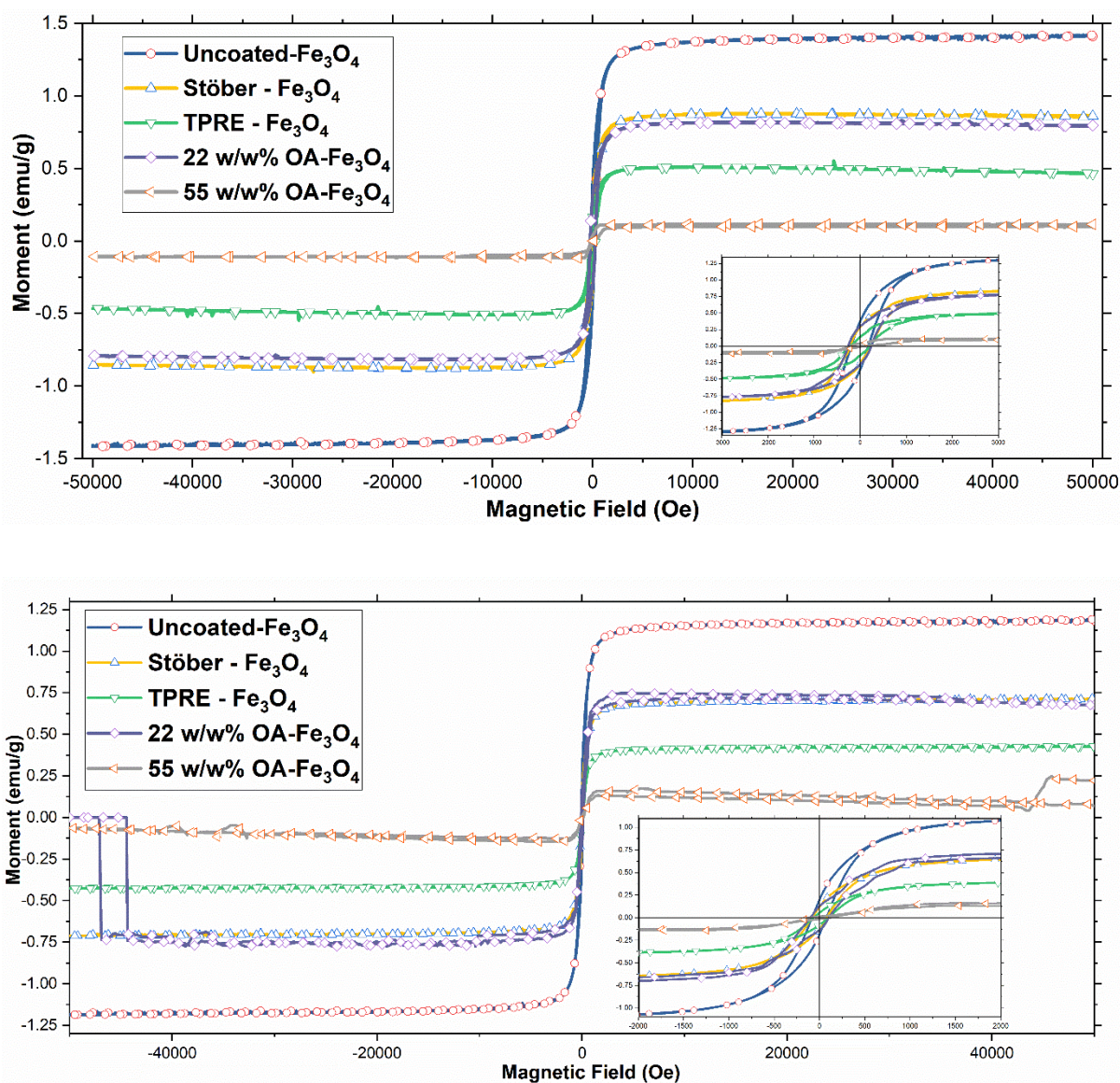
Measurement for MNPs samples-

Figure S2. Magnetisation hysteresis loops for the Uncoated MNPs, MNPs functionalised by Stöber and TPRE method and MNPs functionalised by 22 w/w% and 55 w/w% OA; measured at 100 K and 400 K respectively from above.

The calculated values from the plots are summarised as follows in Table S4 and S5:

Table S4: Summarised magnetic results at 100 K for uncoated MNPs and MNPs with varying percentages of silica (Stöber and TPRE) coatings.

Sample	Coercivity (H_c) (Oe)	Magnetic Remanence (M_r) (emu/g)	Magnetic Saturation (M_s) (emu/g)	Magnetic Moment Ratio (M_r/M_s)
Uncoated-Fe$_3$O$_4$ MNPs	166	3682 x 10^{-4}	13280 x 10^{-4}	0.28 ± 0.05
Stöber- Fe$_3$O$_4$ MNPs	209	2811 x 10^{-4}	8482 x 10^{-4}	0.33 ± 0.03
TPRE- Fe$_3$O$_4$ MNPs	210	1370 x 10^{-4}	5069 x 10^{-4}	0.27 ± 0.06
22 w/w% OA-Fe$_3$O$_4$ MNPs	249	2998 x 10^{-4}	7837 x 10^{-4}	0.38 ± 0.03

| 55 w/w% OA-Fe$_3$O$_4$ MNPs | 329 | 775 x 10^{-4} | 2361 x 10^{-4} | 0.33 ± 0.06 |

Table S5: Summarised magnetic results at 400 K for uncoated MNPs and MNPs with varying percentages of silica (Stöber and TPRE) coatings.

| Sample	Coercivity (H$_c$) (Oe)	Magnetic Remanence (M$_r$) (emu/g)	Magnetic Saturation (M$_s$) (emu/g)	Magnetic Moment Ratio (M$_r$/M$_s$)
Uncoated-Fe$_3$O$_4$ MNPs	84	2013 x 10^{-4}	6600 x 10^{-4}	0.12 ± 0.04
Stöber- Fe$_3$O$_4$ MNPs	81	1025 x 10^{-4}	6512 x 10^{-4}	0.16 ± 0.03
TPRE- Fe$_3$O$_4$ MNPs	81	509 x 10^{-4}	3792 x 10^{-4}	0.13 ± 0.05
22 w/w% OA-Fe$_3$O$_4$ MNPs	109	1594 x 10^{-4}	6715 x 10^{-4}	0.24 ± 0.02
55 w/w% OA-Fe$_3$O$_4$ MNPs	109	329 x 10^{-4}	1500 x 10^{-4}	0.22 ± 0.04

Measurements for PMC samples-
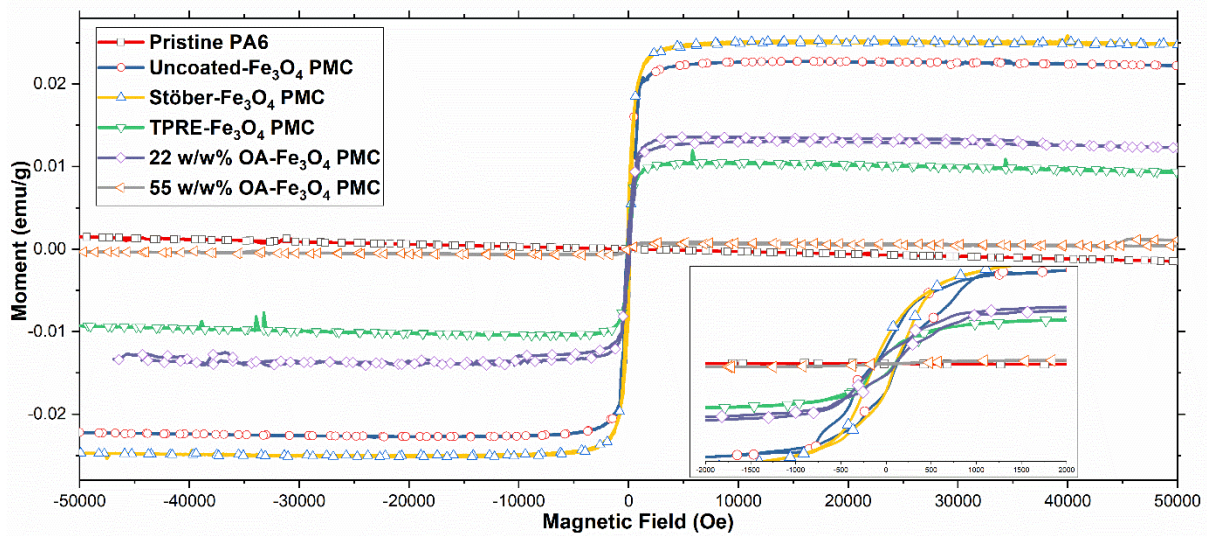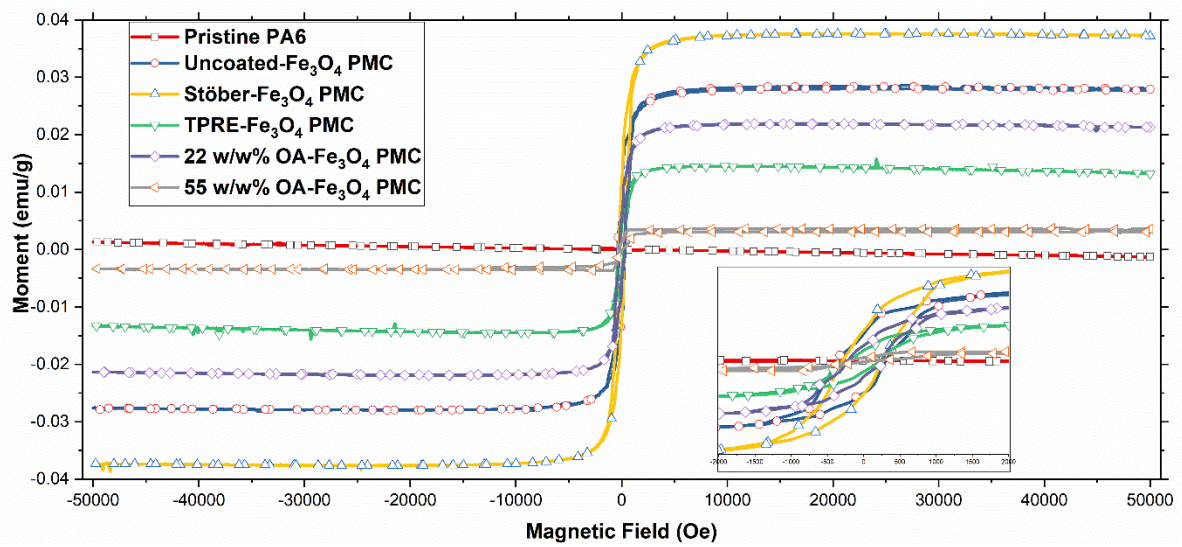
Figure S3: Magnetisation hysteresis loops for the Pristine PA6 sample, PMC sample with uncoated MNPs, PMC samples with varying percentages of silica coatings (Stöber and TPRE) on the MNPs and PMC samples with varying proportions of OA coatings (22 w/w % and 55 w/w%) on the MNPs at 100 K and 400 K respectively.

The calculated values from the plots are summarised as follows in Table S6 and S7:

Table S6: Summarised magnetic results at 100 K for Pristine PA6 sample, sample with uncoated MNPs and samples with varying percentages of silica coatings (Stöber and TPRE) on the MNPs.

| Sample	Coercivity (H_c) (Oe)	Magnetic Remanence (M_r) (emu/g)	Magnetic Saturation (M_s) (emu/g)	Magnetic Moment Ratio (M_r/M_s)
Pristine PA6	0	0	0	0
Uncoated-Fe_3O_4 PMC	360	117×10^{-4}	253×10^{-4}	0.46 ± 0.07
Stöber-Fe_3O_4 PMC	268	126×10^{-4}	336×10^{-4}	0.38 ± 0.03
TPRE-Fe_3O_4 PMC	220	42×10^{-4}	135×10^{-4}	0.31 ± 0.05
22 w/w% OA-Fe_3O_4 PMC	244	63×10^{-4}	200×10^{-4}	0.32 ± 0.04
55 w/w% OA-Fe_3O_4 PMC	362	27×10^{-4}	47×10^{-4}	0.57 ± 0.12

Table S7: Summarised magnetic results at 400 K for Pristine PA6 sample, sample with uncoated MNPs and samples with varying percentages of silica coatings (Stöber and TPRE) on the MNPs.

Sample	Coercivity (H_c) (Oe)	Magnetic Remanence (M_r) (emu/g)	Magnetic Saturation (M_s) (emu/g)	Magnetic Moment Ratio (M_r/M_s)
Pristine PA6	0	0	0	0
Uncoated-Fe_3O_4 PMC	169	82×10^{-4}	211×10^{-4}	0.30 ± 0.06
Stöber-Fe_3O_4 PMC	114	66×10^{-4}	233×10^{-4}	0.28 ± 0.03
TPRE-Fe_3O_4 PMC	109	23×10^{-4}	99×10^{-4}	0.23 ± 0.04
22 w/w% OA-Fe_3O_4 PMC	116	29×10^{-4}	120×10^{-4}	0.24 ± 0.03
55 w/w% OA-Fe_3O_4 PMC	102	3×10^{-4}	9×10^{-4}	0.31 ± 0.09

Section 5 (S5): Simulated Model Generation.

The TEM images of the PMC samples were processed (details in Supplementary Data Section S2) and used for the size inputs for the simulated 3D model using MATLAB® platform and used as the input to the designed MATLAB® code with percentage weight of the NPs loading, to generate the random NP/agglomerates in the simulated nanocomposite 3D model. The code generated the simulated PMC model with the appropriate nanoparticles content and diameter sizes passed as the inputs. The black coloured spheres in the simulated model represent Fe_3O_4 nanoparticles/agglomerates and their interaction region is represented by the grey region around them.

Section 6 (S6): XRD plot for uncoated Fe$_3$O$_4$ nanoparticles.
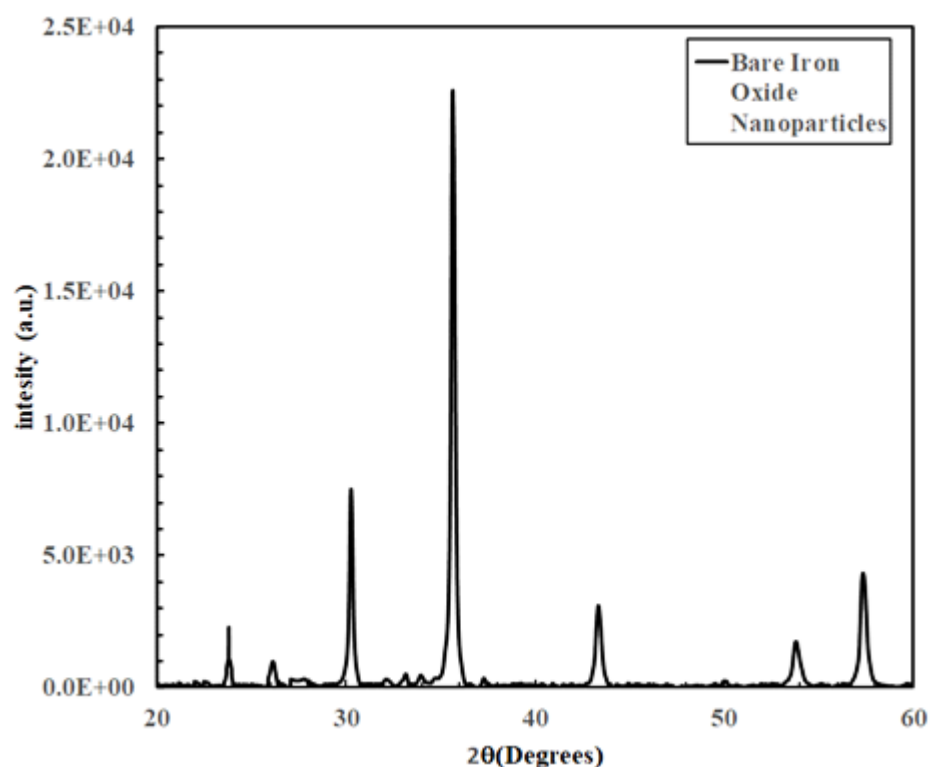
The low value of saturation magnetisation of uncoated iron oxide nanoparticles was due to annealing at temperature above 230°C in air. Before coating with various materials, we wanted to make the nanoparticles free flowing or moisture free. However, it resulted into unintended consequence of generating large amount of haematite phase. Temperature above 230°C can lose oxygen and the small peaks at 23.8,24.1 [1] show the formation of α-Fe2O3, a weak ferromagnetic [2]. The rest of peaks 30.1,35.7, 43.3,53.9, 57.5 belong to Fe$_3$O$_4$[3]. Some small peaks, which are not so visible at 26.2, gave the indication that some carbon powder was mixed with original powder. The resulting mix of α-Fe$_2$O$_3$, Fe$_3$O$_4$ and trace carbon powder might have contributed to the low saturation magnetisation value.

Reference:

(1) Akia, Mandana, K. Andre Mkhoyan, and Karen Lozano. "Synthesis of multiwall α-Fe2O3 hollow fibers via a centrifugal spinning technique." *Materials Science and Engineering: C* 102 (2019): 552-557.

(2) Cao D, Li H, Pan L, Li J, Wang X, Jing P, Cheng X, Wang W, Wang J, Liu Q. High saturation magnetization of γ-Fe2O3 nano-particles by a facile one-step synthesis approach. Sci Rep. 2016 Sep 1;6:32360. doi: 10.1038/srep32360

(3) E. Bertolucci *et al*., "Chemical and magnetic properties characterization of magnetic nanoparticles," *2015 IEEE International Instrumentation and Measurement Technology Conference (I2MTC) Proceedings*, Pisa, Italy, 2015, pp. 1492-1496, doi: 10.1109/I2MTC.2015.7151498